Journal of Chemical Health Risks

www.jchr.org

ORIGINAL ARTICLE

Preparation of a Novel Magnetic Nanocomposite Hydrogel Based on Carboxymethyl Chitosan for the Adsorption of Crystal Violet as Cationic Dye

Meysam Akbarzadeh [1], Mohammad Taghi Vardini*[1], Gholam Reza Mahdavinia [2]

[1]*Department of Chemistry, Tabriz Branch, Islamic Azad University, Tabriz, Iran*

[2] *Department of Chemistry, Faculty of Science, University of Maragheh, Maragheh, Iran*

Received: 22 August 2018 Accepted: 27 October 2018)

KEYWORDS

Crystal Violet (CV);
Carboxymethyl chitosan (CMC);
Magnetic montmorillonite (m-MMT);
Kinetics of adsorption;
Langmuir isotherm

ABSTRACT: The novel magnetic carboxymethyl chitosan/poly (acrylic amide) hydrogel (m-CMC-PAMH) was prepared using magnetic montmorillonite (m-MMT) and characterized by Fourier transform infrared spectroscopy (FT-IR), transmission electron microscopy (TEM), scanning electron microscopy (SEM), X-ray diffraction (XRD) and vibrating sample magnetometry (VSM) techniques. Results showed that m-CMC-PAMH has been prepared successfully properties without damaging the crystal structure of Fe_3O_4. Adsorption capacity of Crystal Violet (CV) on the m-CMC-PAMH was 72.4 mg/g. The CV adsorption well described by the pseudo-second-order kinetics and Langmuir isotherm equations. The positive value of the enthalpy change ΔH° (23.5 kJ/mol) showed that the adsorption was endothermic and physical in nature. The value of Gibbs free energy change ΔG° was found to be -9.7 kJ/mol at 295 K for m-CMC-PAMH, which shows spontaneity of the CV adsorption. So, m-CMC-PAMH can be used as a low-cost alternative to other adsorbents for the removal of dyes from aqueous solutions.

INTRODUCTION

Dyes are widely used in various industries such as leather, textiles, paper, pharmaceuticals and plastics. Unfortunately, the evacuation of them into water, even in small quantities, can affect aquatic life and food chain [1]. The rescue of colored waste from textile plants is unwanted to the environment, not only because of their color but also because of their decay products, many of which are poisonous and mutagenic [2]. Without proper treatment, the dyes are stable and can remain in the environment for a long time. Violet Crystal (CV), an artificial cationic base dye, gives a blue-purple blue to aqueous solutions. CV, typical of triphenyl methane, is widely used in textile industries and is used as a biological element, skin agent, veterinary medicine and animal feed to prevent the spread of harmful bacteria [3]. CV to mammalian cells, as well as mutagen, is a toxic mitosis [4]. Cationic dyes can easily interact with negative cell membrane surfaces and can enter the cells and focus on the cytoplasm. Additionally, they cannot be easily removed by using conventional sewage treatment methods due to their complex structure and their artificial origin [5]. Therefore, the removal of dyes from industrial wastewater is a research discipline that attracts more attention.

A wide range of methods, including electrical coagulation, adsorption, membrane separation, oxidative and biochemical degradations were used to remove cationic dyes from wastewater [6-8]. Among them,

*Corresponding author: mtvardini@iaut.ac.ir (M.T. Vardini)

adsorption has attracted interests in recent years due to low cost, design simplicity, ease of operation and lack of susceptibility to toxins. Many adsorbents, such as activated carbon, zeolite, clay, biomass, polymeric resins, and polymer hydrogels have been investigated [9, 10]. Biodecomposable polymers (synthetic or natural), due to high costs and problems with the regeneration of synthetic polymer sorbents, attract more interests, which has led researchers to concentrate on low-cost alternative natural polymer sorbents [11]. Polysaccharides, such as chitosan and alginate, have been reported [12, 13]. It should be noted that natural adsorbents made of biodegradable polymers are biological and have led to applications in the food and pharmaceutical industries [14].

The promised magnetic separation provides an environmental purification method for the lack of production of pollutants such as flocculants and the ability to deal with large quantities of wastewater in a short time [15]. Magnetic iron oxide, nanoparticles, or micro particles are widely used in separation and adsorption areas, especially in the separation of ion exchange and enzyme, nucleic acid and cell separation [16, 17] and also to remove dyes [18]. Magnetic nanoparticles embedded in porous polymer materials can improve the adsorption capacity due to the expansion of electrostatic interactions. Inflation of the hydrogel allows the cationic dye molecules to penetrate into the hydrogel to adsorb hydrogel adsorbent functional groups. The effect of cationic dye molecules on the hydrogel can be created by electrostatic and hydrophobic interactions between the penetrating molecules and the hydrogel. Therefore, the cationic dye adsorption capacity increases due to electrostatic and hydrophobic interactions. However, well-known, the combination of biodegradable grafted polymer hydrogels with magnetic nanoparticles is not well documented for the removal of cationic dyes in literature.

In the research reported here, we attempted to prepare magnetic nanocomposite hydrogels using an in-situ synthesis of carboxymethyl chitosan/poly(acryl amide) (CMC-PAM) hydrogels in the presence of Fe_3O_4-montmorillonite nanoparticles (m-MMT) via cross-linking graft copolymerization. The magnetic nanocomposite CMC-PAM hydrogels (m-CMC-PAMH) were used to remove and separate CV as a cationic dye from aqueous solutions using the electrostatic interactions between the hydrogels and CV molecules. The swelling behavior and adsorption properties of these magnetic nanocomposite hydrogels in CV solution were also investigated in detail.

MATERIALS AND METHODS

Materials

Acryl amide (AM, as monomer) and carboxymethyl chitosan (CMC, as hydrogel) were purchased from the company of Sigma-Aldrich (USA). Sodium montmorillonite (MMT, as nano-clay) supplied by Rockwood Additives Ltd. (UK). Methylene bis-acrylamide (MBA, as cross-linking agent) and potassium persulfate (KPS, as initiator) were purchased from Fluka and Merck (Germany), respectively. Crystal Violet (CV, as cationic dye) with formula of $C_{25}H_{30}NCl$ and molar weight of 407.95 g/mol was obtained from Sigma-Aldrich (USA) (Figure 1). Other chemical agents used were all analytical grade and all solutions were prepared with double distilled water.

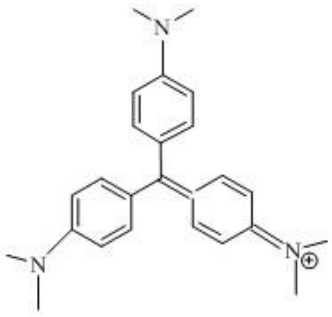

Figure 1. Structure of Crystal Violet (CV).

Instruments

The proposed nanoparticles were characterized by Fourier infrared spectroscopy (FT-IR), X-ray diffractometry (XRD), scanning electron microscopy (SEM), transmission electron microscopy (TEM) and magnetization measurements by vibrating sample magnetometry (VSM).

The FT-IR spectrum was recorded on a Fourier-transform Infrared Spectrometer Bruker in KBr disc. The crystallographical structures of nanocomposites were determined using an X-ray diffractometer (Siemens D-500). The diffraction data were collected from 2θ = 1-80°. The surface morphology of the synthesized nanocomposites was examined using a scanning electron microscope of Vega-Tescan. The microstructure of nanoparticles was characterized using a transmission electron microscope of Philips CM10. The magnetization measurements were carried out at room temperature using a vibrating sample magnetometer of Lakeshare 7400 in a field ranging from -10 to +10 kOe. The dye concentrations were measured at a wavelength λ = 595 nm by UV-Vis Shimadzu 1700 spectrophotometer.

Preparation of m-CMC-PAMH nanocomposites

To prepare the m-CMC-PAAH nanocomposites, the preparation procedure was separated into two stages. The first stage was to prepare magnetic nano-clay. In order to magnetization of MMT nano-clay, 3 g of clay was dispersed in 200 ml of distilled water for 10 min using ultrasonic bath (30 kHz). At the same time, 3 g of $FeCl_3$,$6H_2O$ and 1.9 g of $FeSO_4$,$7H_2O$ were dissolved in 20 ml of distilled water and immediately added into MMT clay suspension under temperature 70 °C. Then the pH of this mixture was regulated in 10 with ammonia solution and after 1 h stirring, magnetic nano-clay particles separated by the external magnet. In order to neutralize the pH of resulting m-MMT, it was washed several times by distilled water and in this way; finally the desired nano-clay was obtained for the preparation of m-CMC-PAAH nanocomposite hydrogels.

In the second stage of the m-CMC-PAMH nanocomposite preparation, CMC solution was obtained by dissolving 0.75 g of CMC in 30 ml distilled water. The certain weight of resulting m-MMT was then added to the prepared CMC solution. The mixture temperature was raised to 70 °C under continuous stirring for 30 min. 3 g AM and 0.03 g MBA dissolved in 2 ml of distilled water were added over the reaction mixture and subjected in ultrasonic condition (30 kHz) for a minute. After one hour stirring, 0.1 g KPS dissolved in 2 ml of distilled water was added to the reaction mixture and after the formation of magnetic nanocomposite hydrogel; it was transferred to the plate in an oven and dried at 60 °C. Finally the synthesized m-CMC-PAAH nanocomposite was ground, meshed and kept away from moisture and light. It is worth noting the 60 mesh was used in all tests.

Swelling studies

To evaluate the swelling behavior of the proposed hydrogel in distilled water, salt and aqueous solutions with different pH values, the amount of 0.1 g nanocomposite hydrogels were poured into desired solutions and let swell for 24 h. After this period, the samples were filtered and the swelling ratio measured using the following equation:

$$SR = (W_s-W_d)/W_d \qquad (1)$$

Where W_d and W_s are the weight of used hydrogel in the dry and swollen state, respectively.

Adsorption studies

To study the kinetics of adsorption, 0.1 g of dry samples were poured in 50 ml of cationic dye solution (CV, 50 ppm) and stirred on a shaker at 120 rpm in ambient temperature and the absorbance values of solutions measured at different intervals with UV-Vis spectrophotometry (λ_{max} = 595 nm). The amount of CV adsorption at the moment t, q_t (mg/g), was calculated from equation 2:

$$q_t = (C_0-C_t)\ V/W \qquad (2)$$

Here, C_0 and C_t were the initial and moment t concentration of CV (ppm); V and W were the volume of solution (L) and weight of magnetic nanocomposite hydrogel samples (g), respectively.

In order to investigate the isotherm of CV adsorption, 0.05 g of the synthesized hydrogels were poured in 50 ml of CV solutions with concentrations of 25, 50, 75, 100, 150 and 200 ppm and stirred for 24 h on shaker with speed 120 rpm at room temperature. The initial and final CV concentrations measured by UV-Vis spectrophotometry at wavelength of 595 nm using calibration curve and equilibrium adsorption capacities, q_e (mg/g), were calculated from equation 2.

RESULTS AND DISCUSSION

In this work, the magnetic nanocomposite hydrogel was synthesized from the grafting of AM monomer on the CMC in the presence of m-MMT. For the cross-linking of the hydrogel, MBA and initiator of KPS were used. In the first stage, MMT was magnetized in the presence of iron (II) and iron(III) and after purification; it was used to prepare the magnetic nanocomposites. Thermal initiator of persulfate was heated to become the sulfate anion-radicals that pull hydrogen radicals from the carboxymethyl chitosan. Therefore, acryl amide monomer grafted onto the biopolymer and a cross-linked copolymer was obtained due to the presence of cross-linking agent. Thus, m-MMT will be involved in the network [19]. A simple representation of the preparation polymerization was shown in Figure 2.

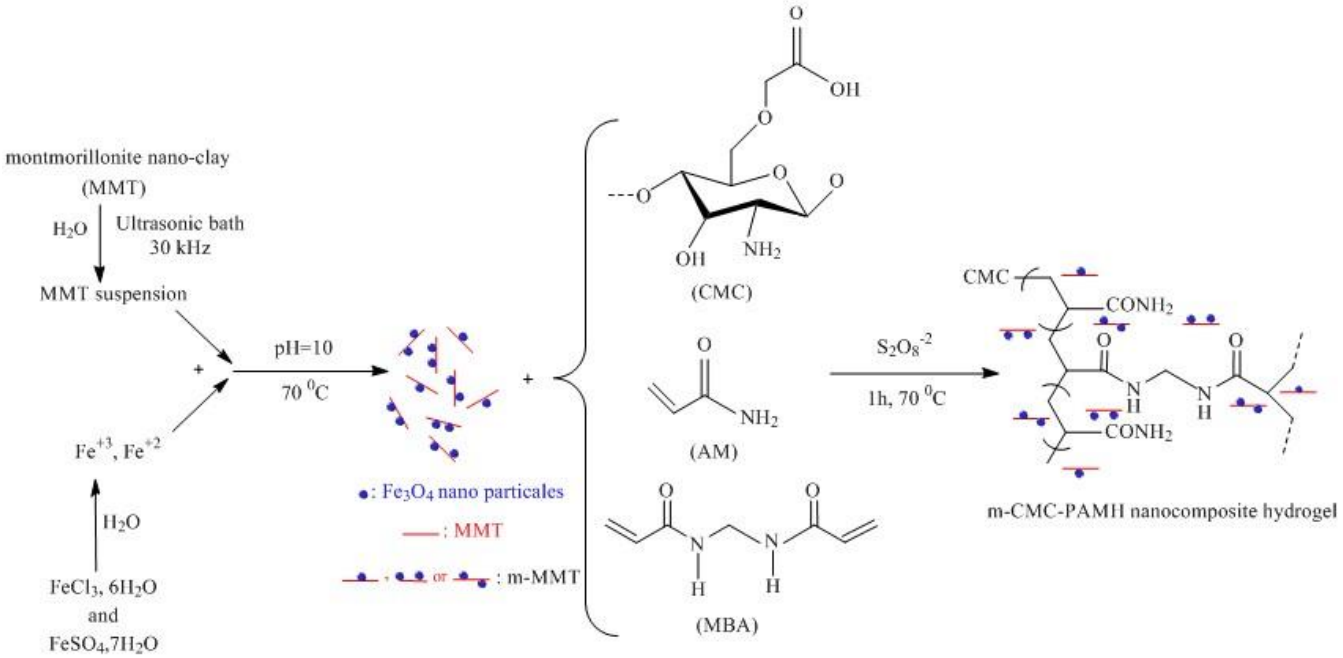

Figure 2. Scheme for the preparation procedure to proposed adsorbent of m-CMC-PAMH nanocomposite hydrogel.

Structural characterization

FT-IR analysis

Figure 3 shows FT-IR spectra of MMT (Figure 3a), m-MMT (Figure 3b), CMC (Figure 3c), CMC-PAMH (Figure 3d) and m-CMC-PAMH (Figure 3e). The stretching vibrations of C-H bond in $-CH_2$ are located at around 2925 cm^{-1} and in $-CH_3$ group are located at 2854 cm^{-1} (CMC, CMC-PAMH and m-CMC-PAMH) [20, 21]. Bending vibrations of methylene and methyl groups are located at 1385, 1431 cm^{-1} for the CMC, 1385, 1418 cm^{-1}

for the CMC-PAMH and 1385, 1415 cm^{-1} for the m-CMC-PAMH, respectively. The CMC, CMC-PAMH and m-CMC-PAMH spectra present bands respectively at around 1615, 1601 and 1594 cm^{-1} corresponding to the C=O bond of the carboxymethyl group. These shifts on carbonyl groups of CMC-PAMH and m-CMC-PAMH to lower frequencies were probably due to inter- and/or intramolecular interactions between CMC and PAM through both hydrogen bonding [22] and covalent bonding [23, 24]. The CMC-PAMH and m-CMC-PAMH spectra had broad bands respectively around 3283 and 3449 cm^{-1} due to the stretching vibration of N-H. The significant characteristic peak at around 1385 cm^{-1} was attributed to the C-N stretching vibration (Figure 3d and Figure 3e) [25].

The strong bands located at around 1043 cm^{-1} (Figure 3a, MMT), 1008 cm^{-1} (Figure 3b, m-MMT) and 1115 cm^{-1} (Figure 3e) refer to Si-O-Si moiety and stem from stretching. The bands at around 524, 533 and 637 cm^{-1} respectively for the MMT, m-MMT and m-CMC-PAMH indicate bending vibration of Si-O. These peaks for MMT are confirmed in literature [26]. The bands at 708 cm^{-1} for the m-MMT and 710 cm^{-1} for the m-CMC-PAMH can be attributed to the Fe-O bond [27].

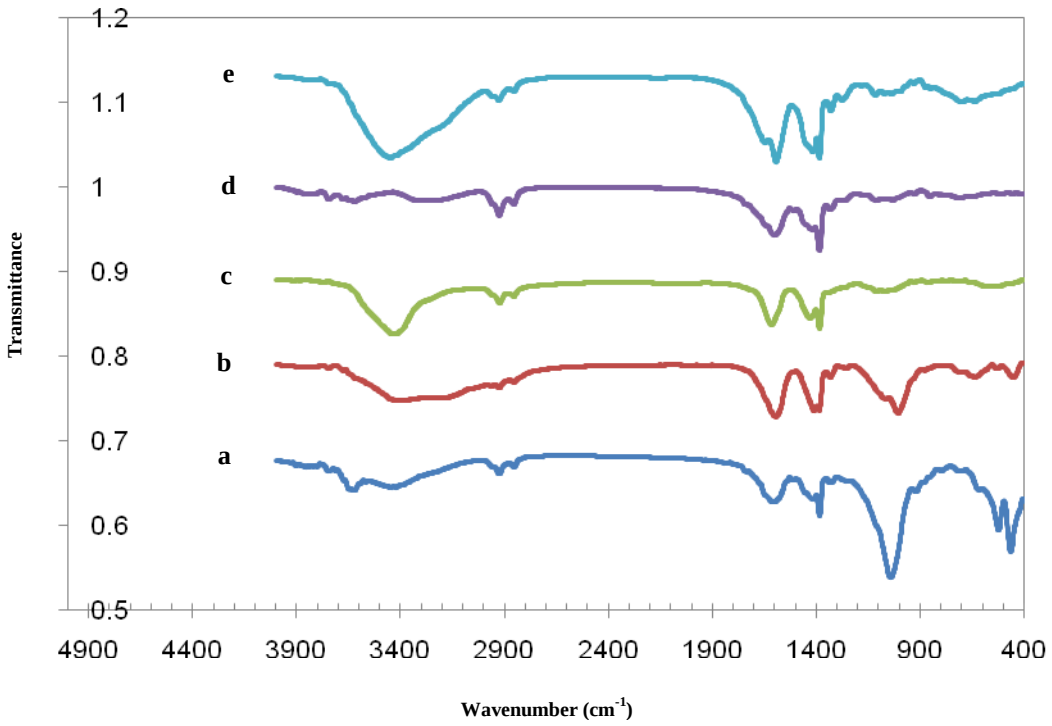

Figure 3. FT-IR spectra of (a) MMT, (b) m-MMT, (c) CMC, (d) CMC-PAMH and (e) m-CMC-PAMH (20% m-MMT).

XRD analysis

In order to study the dispersion type of nanoparticles in the nanocomposite hydrogel matrix X-ray diffraction patterns were used. Figure 4 shows the XRD spectra of raw MMT, m-MMT and m-CMC-PAMH, respectively. As is clear, MMT shows a characteristic peak at $2\theta = 7.5$ that indicate the distance of plates is about 11.61 nm. XRD spectrum corresponding to m-MMT was shown in Figure 4b. As it stands, the characteristic peak at $2\theta = 7.5^{\circ}$ of raw MMT was disappeared. This phenomenon is related to the influence of positioning of iron ions between layers of MMT that Fe_3O_4 magnetic particles are placed between the layers and results in delaminating of MMT. Characteristic peaks at $2\theta = 30.5$, 36, 57.2, and 63.5° indicate that the magnetic nanoparticles were formed [28]. XRD spectrum of m-CMC-PAMH nanocomposite hydrogel was shown in Figure 4c. As it is clear, the characteristic peak at $2\theta = 7.5^{\circ}$ of MMT was vanished. The characteristic peaks at $2\theta = 30.5$, 36, 57.2, and 63.5° are existence evidence of the magnetic nanoparticles in hydrogel matrix.

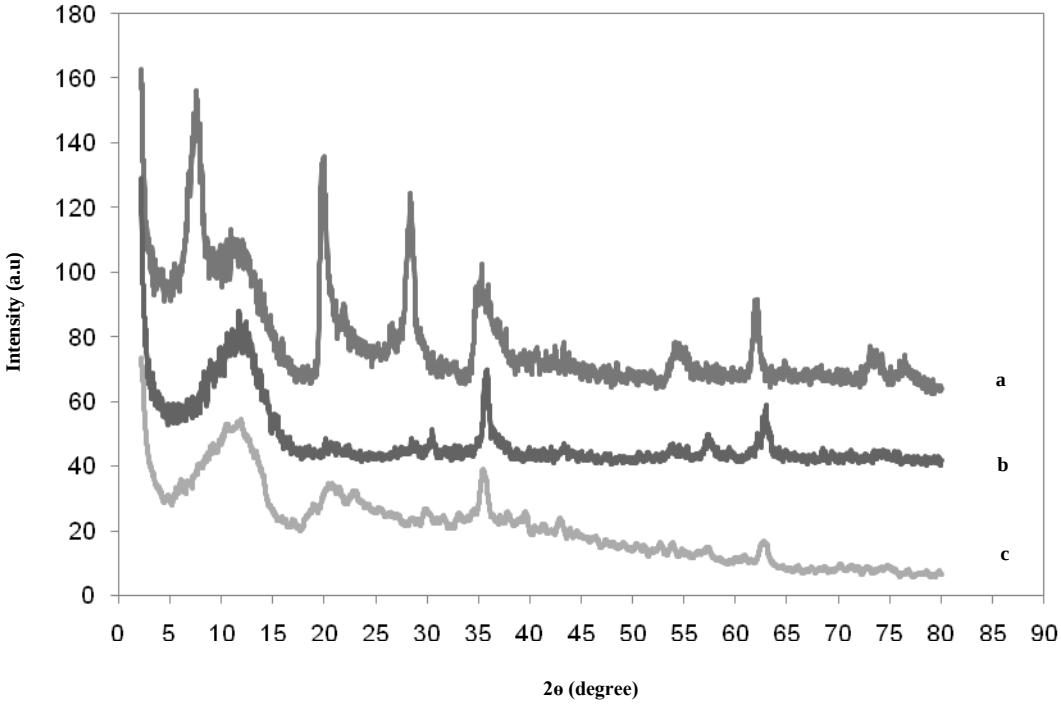

Figure 4. XRD patterns of (a) MMT, (b) m-MMT and (c) m-CMC-PAMH (20% m-MMT).

Study of surface morphology

To survey the surface of hydrogels, the SEM images were used. SEM images related to CMC-PAMH and m-CMC-PAMH hydrogels were shown in Figure 5a to Figure 5c, respectively. As is clear from the image of CMC-PAMH, an almost smooth surface has been achieved. With the introduction of m-MMT nanoparticles into hydrogel structure, hydrogel surface was changed and uneven surface obtained. This rough surface was due to the presence of magnetic montmorillonite.

TEM micrograph

Micrograph related to TEM of m-CMC-PAMH nanocomposite hydrogel sample was studied. The image for TEM micrograph of the proposed sample was shown in Figure 6. Fe_3O_4 nanoparticles are stuck as spherical particles between the montmorillonite fibers. This image shows well the formation of magnetic nanoparticles in the presence of montmorillonite. Montmorillonite fibers are also in the hydrogel matrix in dimensions less than 100 nm.

Magnetic characterization

To check the saturation magnetization of the synthesized samples, vibrating magnetometry spectra were used. Spectra of the samples are shown in Figure 7. As it stands, saturation magnetization of the m-CMC-PAMH (10% Fe_3O_4) is half of the m-CMC-PAMH (20% Fe_3O_4) sample which is in accordance with the amount of m-MMT used for synthesis of nanocomposite hydrogels. The saturation magnetization was enough to use a magnet for separation of nanocomposites from the operating environment.

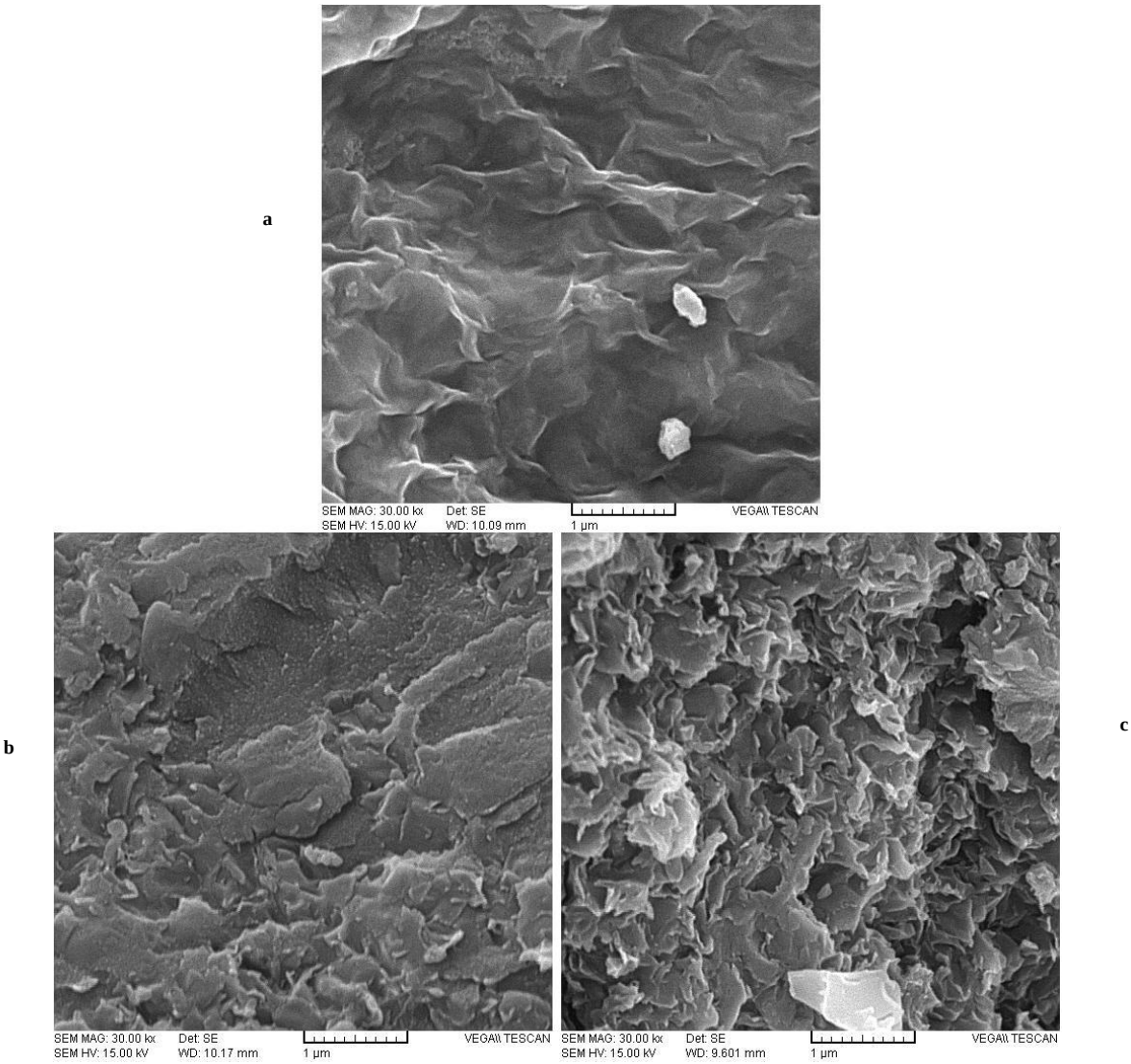

Figure 5. SEM images of (a) CMC-PAMH, (b) m-CMC-PAMH (10% m-MMT) and (c) m-CMC-PAMH (20% m-MMT).

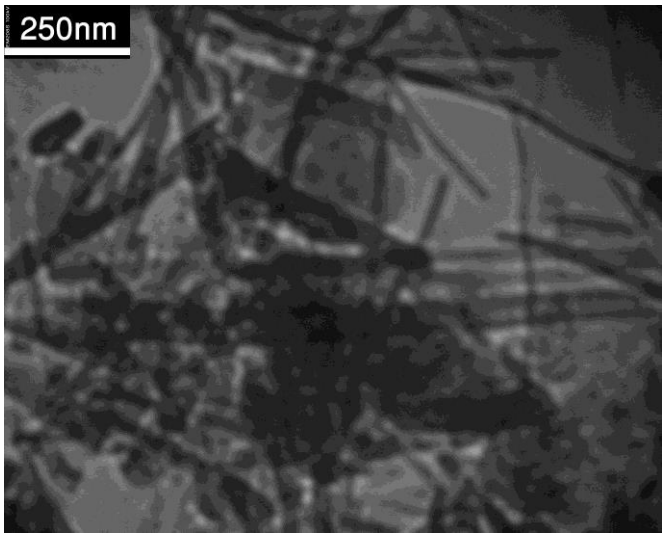

Figure 6. TEM micrograph of m-CMC-PAMH nanocomposite hydrogel (20% m-MMT).

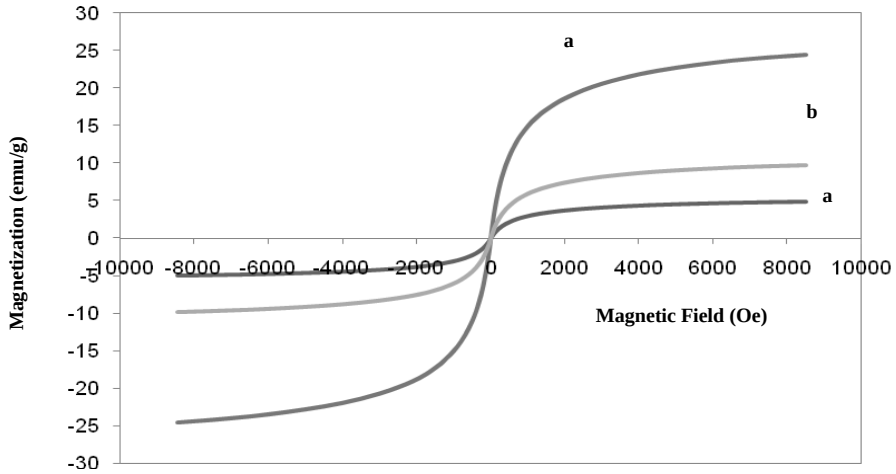

Figure 7. Magnetization curves of (a) m-MMT, (b) m-CMC-PAMH (20% m-MMT) and (c) m-CMC-PAMH (10% m-MMT).

Swelling studies

To investigate the amount of water adsorption by the proposed hydrogels, the swelling of the samples were checked in distilled water, salt solutions and in different pHs. Figure 8 shows the swelling degree (ratio) of the proposed nanocomposite samples in distilled water, sodium chloride (NaCl) and calcium chloride ($CaCl_2$) salt solutions with concentrations of 0.15 M. As is evident from Figure 8, the water adsorption amount of hydrogels decreased with the introduction of m-MMT into their structure. The most important cause of low swelling ratio of the m-CMC-PAMH nanocomposite hydrogels toward hydrogels without nanoparticles can be related to the performance of nanoparticle as a physical network-making. In fact, the physical interactions of the hydrogen bonds between the nanoparticles and hydrogel leads to physical networking and thus pore size and swelling degree is reduced [29].

The swelling ratio of the synthesized hydrogels in salty environments was less than distilled water. Such decrease can be seen in ionic hydrogels. In this project, studied hydrogels were included the carboxymethyl chitosan containing carboxylate anions. When desired hydrogel is placed in salt environments; firstly, the osmotic pressure difference between the solution and the hydrogel was low and subsequently the swelling degree will be reduced. Secondly, anionic groups surrounded by salt cations and thus the repulsion between the anionic groups will be reduced, resulting in low water adsorption. It is noteworthy that swelling ratio in calcium chloride solution was less than sodium chloride environment. This observation is due to the complexation of calcium ions with carboxylate groups, which increases the networking density and thereby water adsorption will be diminished [19].

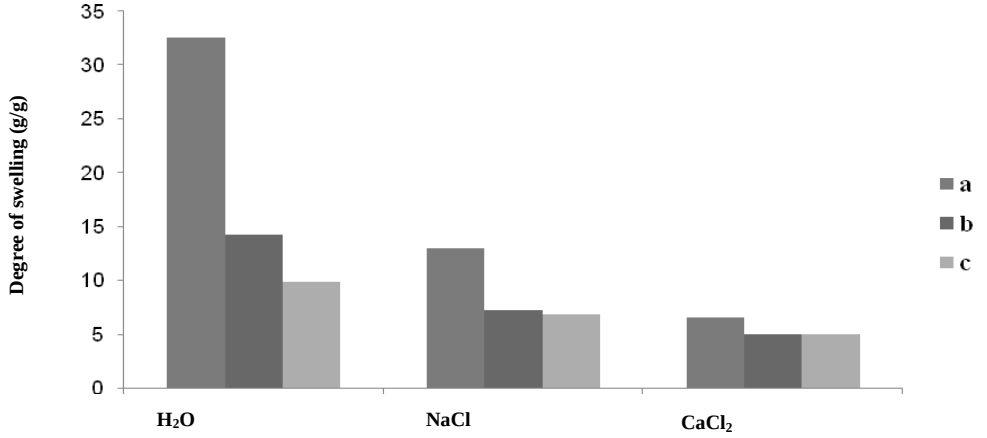

Figure 8. Swelling ratios of the (a) CMC, (b) m-CMC-PAMH (10% m-MMT) and (c) m-CMC-PAMH (20% m-MMT) in distilled water, NaCl and $CaCl_2$ solutions with concentrations of 0.15 M.

Another important factor in swelling behavior of the hydrogels is environment pH (Figure 9). In the structure of the proposed hydrogels, there are 1˚ amine and carboxylate groups in the chitosan chains. The pK_a values for amine and carboxylate groups are around 6.5 and 4.5, respectively. In acidic condition and pHs less than 4.5, carboxylate and amine groups are protonated and therefore can be formed as carboxylic acid (-COOH) and ammonium (NH_4^+). In this pH range, hydrogel shows the swelling behavior that resulted from electrostatic repulsion between ammonium groups on the chitosan ($-NH_3^+.....NH_3^+-$). In the highly acidic pHs, water adsorption of hydrogel is low due to the screening effect. At pH 4 maximum swelling degree may be due to protonation of almost all the amine groups on the chitosan branches. After this maximum water adsorption, reduced swelling ratio can be seen. In this pH range of reduced swelling ratio (4<pH<5.5), fewer amine groups are protonated and the number of cationic groups to electrostatic repulsion is reduced. In addition the carboxylate groups began to dissociate and physical type Cross bonds is created by electrostatic forces between ammonium and carboxylate groups on the network, and by the creation of hydrogen bonds between the amine and carboxylic acid groups (-COO…H...NH_2-). As a result, high networking density and decrease in water adsorption can be seen. After pH 5.5, again increased water adsorption was observed and reached to a maximum value at pH 7. In fact, the number of protonated amine groups is decreased and the number of carboxylate groups added. Thus, the number of cross bonds is reduced and the increase of swelling ratio can be seen. At pH 7, all amine groups are free (-NH_2) and almost all the carboxylic acid groups are dissociated to carboxylate ions [30].

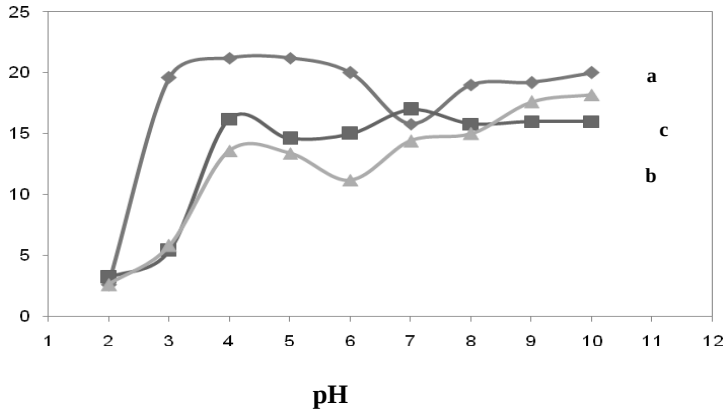

Figure 9. Effects of the amount of environment pH on the swelling ratio of the (a) CMC, (b) m-CMC-PAMH (10% m-MMT) and (c) m-CMC-PAMH (20% m-MMT).

Effect of pH value on CV adsorption

One of the most important factors in dye adsorption is value of solution pH. The pH of solution can affect active centers of the adsorbent and thus dye adsorption on the adsorbent will be affected by the changes of its surface. For this purpose, pH of primary CV solutions was changed in the range of 2 to 10 and results shown in Figure 10. As is obvious, at acidic pHs, the amount of CV adsorption is low. This result is consistent with the swelling behavior of hydrogels at different pHs. At acidic pHs, anionic carboxylate groups are protonated and thus active centers will be decreased. Also, the results indicate that the introduction of m-MMT has improved the amount of adsorption in acidic environments which is similar to the results of our previous work on CarAlg-MMT nanocomposite [13]. In fact, counteraction of m-MMT to the environment pH is not such as CMC.

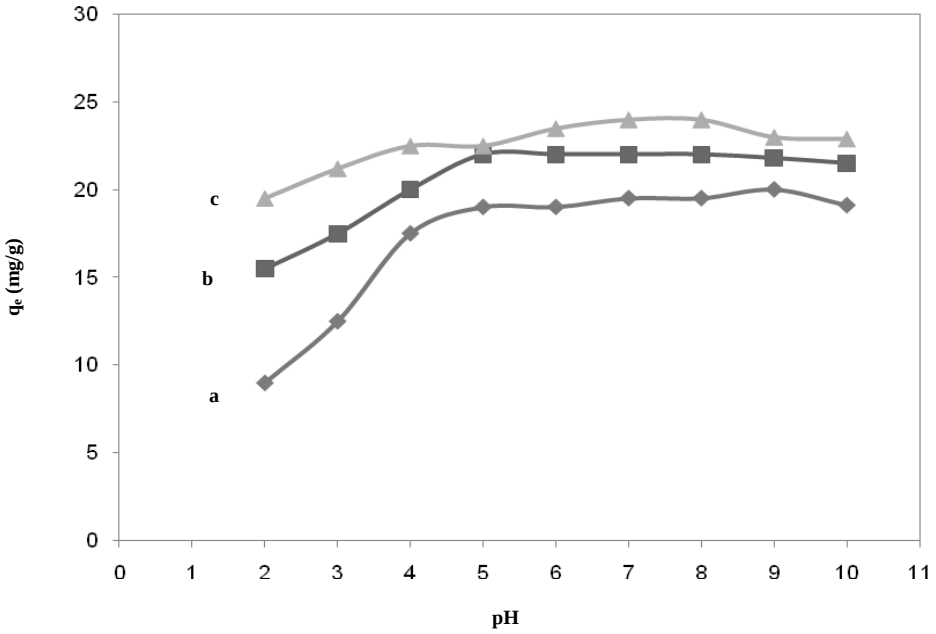

Figure 10. Effects of pH on CV adsorption capacity of (a) CMC, (b) m-CMC-PAMH (10% m-MMT) and (c) m-CMC-PAMH (20% m-MMT).

Effect of ion strength on the adsorption capacity

As was clear from data of swelling related to synthesized hydrogels, swelling behavior was affected by the ionic strength of environment (Figure 8). As water adsorption of hydrogels was lower in salt solutions. It was also reported that dye adsorption reduced for the adsorbents containing hanging anionic groups. For this purpose, we tried to review the adsorption of CV solutions that their ionic strengths were set by different concentrations of NaCl. The concentration of sodium chloride was changed from 0.01 to 0.5 M and the results shown in Figure 11. As the results show CV adsorption onto adsorbent decreases with increasing salt concentration. This data is consistent with the results of swelling behavior in the salty environments. In fact, in such solutions water adsorption of adsorbents was lower and thus reduced its surface, subsequently the number of active centers reduced [31].

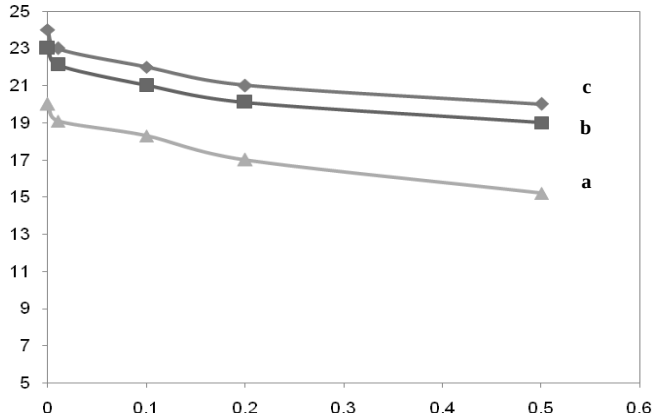

Figure 11. Dependence of CV adsorption on the (a) CMC, (b) m-CMC-PAMH (10% m-MMT) and (c) m-CMC-PAMH (20% m-MMT) as a function of the NaCl concentration.

Adsorption kinetics

Adsorption kinetics offers useful information including the time to reach equilibrium of CV adsorption on the adsorbent. Figure 12 shows CV adsorption capacity of synthesized hydrogels toward time. As it stands, CV adsorption capacity increased with time and then remained constant. Equilibrium time for all proposed samples was approximately 100 min. Rapid adsorption of CV dye in early times could be related to the high number of active centers that after a while these centers are saturated and therefore CV adsorption capacity remains constant. As is evident from the Figure 12, with the presence of m-MMT in the hydrogel structure adsorption capacity of the adsorbent somewhat improved. This improvement could be due to adsorbent surface. According to SEM images, with the introduction of m-MMT adsorbent surface has become from smooth to rough and relatively porous state. These pores increase the adsorbent surface and thus active centers to CV adsorption augmented [13].

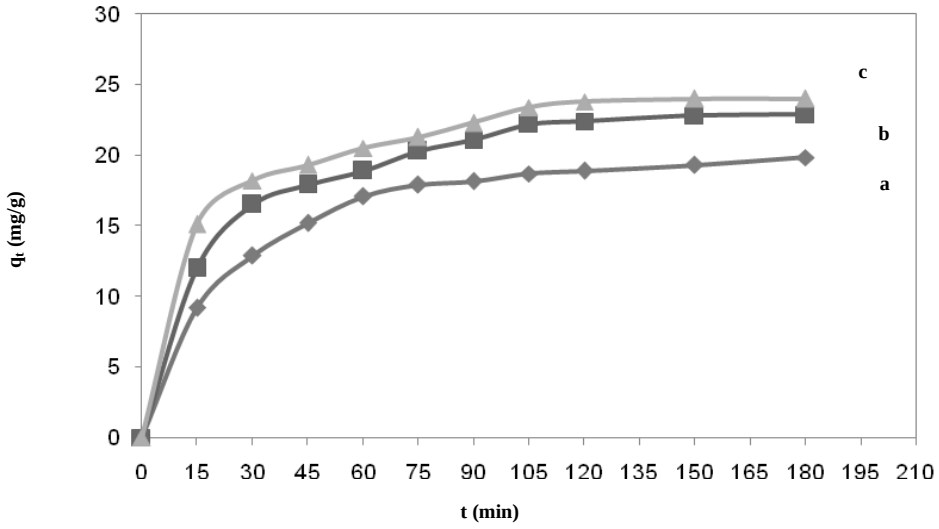

Figure 12. Adsorption kinetics of (a) CMC, (b) m-CMC-PAMH (10% m-MMT) and (c) m-CMC-PAMH (20% m-MMT).

For the detailed review of kinetics for the CV adsorption on the synthesized adsorbents, the adsorption kinetics equations of pseudo-first and pseudo-second order were used. It is worth noting that the non-linear equations used in this project. The pseudo-first order equation was shown in relation 3 [32]:

$$q_t = q_e(1-e^{-k_1 t}) \qquad (3)$$

In this equation, q_t, is the amount of CV adsorption capacity in time t, and q_e, is the equilibrium adsorption capacity that can be calculated theoretically. Constant of k_1 is the rate constant of pseudo-first kinetics. The pseudo-second order equation was shown in relation 4 [32]:

$$q_t = \frac{q_e^2 k_2 t}{1+q_e k_2 t} \qquad (4)$$

Where, q_t, is the CV adsorption capacity at time t, and q_e, is the amount of equilibrium adsorption capacity that can be calculated by the pseudo-second equation after modeling. Constant k_2 is the rate constant related to the pseudo-second kinetics.

To check which model is consistent with experimental results and expressed the adsorption kinetics, the Chi-square test (χ^2) according to the equation 5 and the coefficient of determination (r^2) according to the equation 6 were used [33]:

$$\chi^2 = \sum_{i=1}^{n} \frac{(q_{i,cal.} - q_{i,\exp.})^2}{q_{i,\exp.}} \qquad (5)$$

$$r^2 = \frac{(q_{i,\exp.} - \bar{q}_{i,cal.})^2}{\sum_{i=1}^{n} (q_{i,\exp.} - \bar{q}_{i,cal.})^2 + (q_{i,\exp.} - q_{i,cal.})^2} \qquad (6)$$

Here, $q_{i,exp.}$ and $q_{i,cal.}$, are the practical and theoretical CV adsorption capacities, respectively and $\bar{q}_{i,cal.}$ is the average of theoretical adsorption capacities. The smaller value of χ^2 shows compatibility of the used model with experimental results. Moreover, if the r^2 is close to 1 indicates the model is better consistent with experimental results. Values of constants related to the pseudo-first and pseudo-second order equations are shown in Table 1. Conformity of the experimental results with kinetic models is also shown in Table 1. As is clear from the Table 1, in all three synthesized hydrogels, adsorption of CV onto absorbents followed from the pseudo-second kinetics equation. Also according to Table 1, χ^2 values for pseudo-second equation were lowest amounts that suggest the experimental data followed the pseudo-second kinetics. The r^2 values while confirmed this subject. Also, experimental and theoretical values of CV adsorption capacities for the adsorbents were equal.

Table 1. The rate constants, calculated q_e, Chi-square test and the determination coefficients of two studied kinetic models related to the CV adsorption onto m-CMC-PAMH nanocomposite hydrogels

	Pseudo-first order				Pseudo-second order				
Adsorbent	k_1 (1/min)	q_e (mg/g)	χ^2	r^2	k_2(g/mg.min)	q_e (mg/g)	χ^2	r^2	$q_{e,\ exp.}$ (mg/g)
CMC	0.047	26	1.450	0.85	2.2	22.3	0.30	0.99	19.85
m-CMC-PAMH (with 10% m-MMT)	0.035	18	1.048	0.81	2.3	25.2	0.25	0.98	22.9
m-CMC-PAMH (with 20% m-MMT)	0.038	20	0.660	0.82	3.3	25.4	0.08	0.98	24

Equilibrium studies

Equilibrium adsorption isotherm is of fundamental importance in the design of adsorption system. Distribution of CV dye in equilibrium between the solution liquid and adsorbent solid phases expressed by Langmuir and Freundlich adsorption isotherm models. These equations has been widely used, initially were purely empirical, but recently assumed that the highest amount of adsorption occurs when the surface of adsorbent is covered by the functional groups.Langmuir isotherm model is valid to monolayer adsorption on a surface that has finite number of same adsorption sites, and is displayed as the following equation [34]:

$$q_e = \frac{q_m K_L C_e}{1 + K_L C_e} \qquad (7)$$

Where C_e is the equilibrium concentration (ppm), q_e, is the amount of equilibrium adsorption capacity (mg/g), and q_m, K_L are the Langmuir constants related to the adsorption capacity and energy, respectively. Freundlich model that reflects the heterogeneous surface of adsorbent is given by the following equation [34]:

$$q_e = K_F C_e^{1/n} \qquad (8)$$

That K_F and 1/n are the Freundlich constants related to the adsorption capacity and intensity, respectively.

Table 2 shows the isotherm parameters of CV adsorption onto the synthesized adsorbents. These curves indicate compliance of empirical data with the Langmuir equation. Isotherm constants of CV adsorption on the proposed hydrogels are shown in Table 2. As is clear from the data in Table 2, the least amount of Chi-square test (χ^2) obtained for Langmuir model that represents the practical data followed the Langmuir model. The coefficient of determination (r^2) in this model is close to 1 and also the maximum amount of experimental and theoretical isotherm adsorptions are close to one another in Langmuir model.

Table 2. Freundlich and Langmuir parameters for adsorption of CV on the m-CMC-PAMH nanocomposite hydrogels

Adsorbent	Freundlich model				Langmuir model				
	n (g/L)	K_F (mg/g)(L/mg)$^{1/n}$	χ^2	r^2	q_m (mg/g)	K_L (L/mg)	χ^2	r^2	$q_{m,exp.}$
CMC	2.38	10.12	0.63	0.81	63.9	0.045	0.19	0.99	60.5
m-CMC-PAMH (with 10% m-MMT)	2.96	18.48	0.56	0.85	69.8	0.14	0.024	0.97	68.5
m-CMC-PAMH (with 20% m-MMT)	3.05	21.30	0.68	0.80	74.7	0.174	0.07	0.97	72.4

Thermodynamic parameters

The process of adsorption onto adsorbent material was happened spontaneously or not, as well as being endothermic or exothermic process of adsorption can be achieved by thermodynamic relations. Gibbs free energy (ΔG, kJ/mol), enthalpy (ΔH, kJ/mol), and entropy (ΔS, J/mol.K) are obtained from the following relations [35]:

$$K_D = \frac{C_d}{C_e} \qquad (9)$$

$$\Delta G = -RT \ln K_D \qquad (10)$$

$$LnK_D = \frac{\Delta S}{R} - \frac{\Delta H}{RT} \qquad (11)$$

Where K_D is the equilibrium constant; C_d, C_e (ppm) are the adsorbed (onto adsorbent) and remained equilibrium (in solution) dye concentrations, respectively. R is universal gas constant (8.314 J/mol. K) and T is the absolute temperature (K). By plotting the curve of Ln K_D to 1/T, entropy and enthalpy can be achieved. The values obtained are shown in Table 3. Negative values of Gibbs free energy indicate the spontaneous nature of the CV adsorption on the adsorbent and positive values of enthalpy indicate that the adsorption process is endothermic. Also a positive value for entropy indicates a tendency of hydrogel to CV dye [35].

Table 3. Thermodynamic parameters for the adsorption of CV onto m-CMC-PAMH nanocomposite hydrogel (20% m-MMT)

T (K)	ΔS (J/K.mol)	ΔH (kJ/mol)	ΔG (kJ/mol)	r^2
295			-9.7	
305	+113	+23.5	-10.6	0.95
315			-11.98	

CONCLUSIONS

CV adsorption capacities for the m-CMC-PAMH, as well as its other features are comparable to those of other low-cost adsorbent materials as shown in Table 4. It can be seen from the Table that m-CMC-PAMH showed comparable characteristics with respect to other adsorbent materials. It is clear that m-CMC-PAMH appropriate and promising to removal the CV dye from aqueous solutions. In this research work, magnetic and nanocomposite hydrogel composed of CMC and m-MMT was prepared. The results showed that MMT-clay appears as nano-form in the hydrogel composition. As well as, Fe_3O_4 nanoparticles created spherically in the polymer matrix. Magnetic nano-clay affected on the swelling behavior of hydrogels.

Table 4. The comparison of CV adsorption characteristics of the system reported in this study with adsorbents from the literature

Adsorbent	Optimized Solution pH	Adsorption isotherm model	Adsorption kinetics model	Adsorption capacity (mg/g)	Reference
Jute fiber carbon (JFC)	~ 8	Langmuir	Pseudo-second- order	27.99	[36]
Grapefruit peel	~ 8	Langmuir	Pseudo-second-order	254.16	[37]
Semi-interpenetrated networks hydrogels	~ 7.4	Langmuir	Pseudo-second-order	~ 24.53	[9]
Magnetic nanocomposite	~ 8.5	Langmuir	-	111.80	[18]
Bentonite-FeCo nanocomposite	~ 11	Langmuir and Freundlich	-	13	[38]
Carrageenan-based nanocomposite	~ 7	Freundlich	Pseudo-second-order	30	[39]
CarAlg/MMt nanocomposite hydrogel	~ 6.4	Langmuir	Pseudo-second-order	88.8	[13]
polysaccharide-based magnetic nanocomposite	~ 7	Langmuir	Pseudo-second-order	80.64	[40]
Magnetic k-carrageenan-g-poly(methacrylicacid) nanocomposite	~ 7	Langmuir	Pseudo-second-order	28.24	[11]
Carboxymethyl chitosan-based magnetic nanocomposite	~ 7	Langmuir	Pseudo-second-order	72.4	Present study

As with the introduction of this compound into the matrix of hydrogels, the amount of water adsorption declined. The sensitivity of proposed samples to the pH was also examined which shows the smart-acting of obtained hydrogels. In the adsorption study section, the results showed that the introduction of magnetic nano-clay, CV adsorption capacity of hydrogels increased, which can be due to rough surface of the magnetic hydrogels. The kinetics of CV adsorption onto adsorbents was analyzed using pseudo-first and pseudo-second order kinetics models and pseudo-second order model showed better compatibility with experimental results. The effect of salt and pH on the dye adsorption on the synthesized samples was studied. By increasing the salt concentration, dye adsorption onto the samples was low. The effect of pH also showed that in acidic environments dye adsorption on samples is diminished. The investigation of adsorption isotherms were evaluated by non-linear models of Langmuir and Freundlich model showed compatibility with experimental results.

ACKNOWLEDGEMENTS

The Islamic Azad University, Tabriz Branch, Department of chemistry, Analytical Chemistry laboratory supported this work.

REFERENCES

1. Singh V., Sharma A.K., Sanghi R., 2009. Poly (acrylamide) functionalized chitosan: an efficient adsorbent for azo dyes from aqueous solutions. J Hazard Mater. 166 , 327-335.

2. Chatterjee S., Lee M.W., Woo S.H., 2010 Adsorption of Congo Red by chitosan hydrogel beads impregnated with carbon nanotubes. Bioresour Technol. 101, 1800-1806.

3. Idaka E., Ogawa T., Yatome C., Horitsu H., 1985. Behavior of activated sludge with dyes. Bull Environ. Contam Toxicol. 35, 729-734.

4. He H., Yang S., Yu K., Ju Y., Sun C., Wang L., 2010. Microwave induced catalytic degradation of Crystal Violet in nano-nickel dioxide suspensions. J Hazard Mater. 173, 393-400.

5. Crini G., 2008. Kinetic and equilibrium studies on the removal of cationic dyes from aqueous solution by adsorption onto a cyclodextrin polymer. Dyes Pigm. 77, 415-426.

6. Zahrim A.Y., Tizaoui C., Hilal N., 2011. Coagulation with polymers for nanofiltration pre-treatment of highly concentrated dyes: a review, Desalination. 266, 1-16.

7. Wan Ngah W.S., Teong L.C., Hanafiah M.A.K.M., 2011, Adsorption of dyes and heavy metal ions by chitosan composites: A review, Carbohydr Polym. 83, 1446-1456.

8. Gozmen B., Kayan B., Gizir A.M., Hesenov A., 2009. Oxidative degradations of reactive blue 4 dye by different advanced oxidation methods. J Hazard Mater. 168, 129-136.

9. Li S., 2010, Removal of crystal violet from aqueous solution by sorption into semi-interpenetrated networks hydrogels constituted of poly (acrylic acid-acrylamide-methacrylate) and amylose. Bioresour Technol. 101, 2197-2202.

10. Srinivasan A., Viraraghavan T., 2010. Decolorization of dye wastewaters by biosorbents: a review. J Environ Manage. 91, 1915-1929.

11. Gholami M., Vardini M.T., Mahdavinia G.R., 2016. Investigation of the effect of magnetic particles on the Crystal Violet adsorption onto a novel nanocomposite based on k-carrageenan-g-poly (methacrylic acid), Carbohydr Polym. 136, 772-781.

12. Debrassi A., Correa A.F., Baccarin T., Nedelko N., Slawska-Waniewska A., Sobczak K., 2012. Removal of cationic dyes from aqueous solutions using N-benzyl-O-carboxymethyl chitosan magnetic nanoparticles. Chem Eng J. 183, 284-293.

13. Mahdavinia G.R., Aghaie H., Sheykhloie H., Vardini M.T., Etemadi H., 2013. Synthesis of CarAlg/MMt nanocomposite hydrogels and adsorption of cationic Crystal Violet. Carbohydr Polym. 98, 358-365.

14. Bardajee G.R., Pourjavadi A., Ghavami S., Soleyman R., Jafarpour F., 2011. UV-prepared salep-based nanoporous hydrogel for controlled release of tetracycline hydrochloride in colon. J Photochem Photobiol B. 102, 232-240.

15. Zhu H.Y., Fu Y.Q., Jiang R., Jiang J.H., Xiao L., Zeng G.M., Zhao S.L., Wang Y., 2011. Adsorption removal of Congo Red onto magnetic cellulose/Fe3O4/activated carbon composite: Equilibrium, kinetic and thermodynamic studies. Chem Eng J. 173, 494-502.

16. Sari M., Akgol S., Karatas M., Denizli A., 2006. Reversible immobilization of catalase by metal chelate affinity interaction on magnetic beads. Ind Eng Chem Res. 45, 3036-3043.

17. Akutsu J., Tojo Y., Segawa O., Obata K., Okochi M., Tajima H., 2004. Development of an integrated automation system with a magnetic bead-mediated nucleic acid purification device for genetic analysis and gene manipulation. Biotechnol Bioeng. 86, 667-671.

18. Singh K., Gupta S., Singh A.K., Sinha S., 2011. Optimizing adsorption of Crystal Violet dye from water by magnetic nanocomposite using response surface modeling approach. J Hazard Mater. 186, 1462-1473.

19. Wang L., Wang A., 2007. Removal of Congo Red from aqueous solution using a chitosan/organo-montmorillonite nanocomposites. J Chem Technol Biotechnol. 82, 711-720.

20. Islam A.M., Phillips G.O., Sljivo A., Snowden M.J., Williams P.A., 1997. A review of recent developments on the regulatory, structural and functional aspects of gum Arabic. Food Hydrocolloid. 11, 493-505.

21. Aoki H., Al-Assaf S., Katayama T., Phillips G.O., 2007. Characterization and properties of Acacia Senegal (L.) Willd. Var. Senegal with enhanced properties (Acacia (sen) SUPER GUM™): Part 2-Mechanism of the maturation process. Food Hydrocolloid. 21, 329-337.

22. Said H.M., Alla S.G.A., El-Naggar A.W.M., 2004. Synthesis and characterization of novel gels based on carboxymethyl cellulose/acrylic acid prepared by electron beam irradiation. React Funct Polym. 61, 397-404.

23. Zhai M., Yoshii F., Kume T., Hashim K., 2002. Syntheses of PVA/starch grafted hydrogels by irradiation. Carbohydr Polym. 50, 295-303.

24. Lugao A.B., Malmonge S.M., 2001. Use of radiation in the production of hydrogels, Nucl. Instrum. Methods Phys Res Sect B. 185, 37-42.

25. Spinelli L.S., Aquino A.S., Lucas E., d'Almeida, A.R., Leal R., Martins A.L., 2008. Adsorption of polymers used in drilling fluids on the inner surfaces of carbon steel pipes. Polym Eng Sci. 48, 1885-1891.

26. Bajpai A.K., Shukla S.K., Bhanu S., Kankane S., 2008. Responsive polymers in controlled drug delivery. Prog Polym Sci. 33, 1088-1118.

27. Aoki H., Katayama T., Ogasawara T., Sasaki Y., Al-Assaf S., Phillips G.O., 2007. Characterization and properties of Acacia senegal (L.) Willd. Var. Senegal with enhanced properties (Acacia (sen) SUPER GUM™): Part 5. Factors affecting the emulsification of Acacia Senegal and Acacia (sen) SUPER GUM™. Food Hydrocolloid. 21, 353-358.

28. Tang S.C.N., Lo I.M.C., 2013. Magnetic nanoparticles: Essential factors for sustainable environmental applications. Water Res. 47, 2613-2632.

29. Mahdavinia G.R., Bagheri Marandi G., Pourjavadi A., Kiani G., 2010. Semi-IPN Carrageenan-based nanocomposite hydrogels: synthesis and swelling behavior. J Appl Polym Sci. 118, 2989-2997.

30. Mahdavinia G.R., Zohuriaan-Mehr M.J., Pourjavadi A., 2004. Modified chitosan III, superabsorbency, salt- and pH-sensitivity of smart ampholytic hydrogels from chitosan-g-PAN. Polym Adv Technol. 15, 173-180.

31. Al-Degs Y.S., Barghouthi M.I., El-Sheikh A.H., Walker G.M., 2007. Effect of solution pH, ionic strength, and temperature on adsorption behavior of reactive dyes on activated carbon. Dyes Pigm. 77, 16-23.

32. Ho Y.S., Mckay G., 1999. Pseudo-second order for sorption processes. Process Biochem. 34, 451-465.

33. Foo K.Y., Hameed B.H., 2010. Insights into the modeling of adsorption isotherm systems. Chem Eng J. 156, 2-10.

34. Ho Y.S., McKay G., 2003. Sorption of dyes and copper ions onto biosorbents. Process Biochem. 38, 1047-1061.

35. Liu Y., 2009. Is the free energy change of adsorption correctly calculated?, J Chem Eng Data. 54, 1981-1985.

36. Porkodi K., Kumar K.V., 2007. Equilibrium, kinetics and mechanism modeling and simulation of basic and acid dyes sorption onto jute fiber carbon: Eosin yellow, malachite green and crystal violet single component systems. J Hazard Mater. 143, 311-327.

37. Saeed A., Sharif M., Iqbal M., 2010. Application potential of grapefruit peel as dye sorbent: Kinetics, equilibrium and mechanism of crystal violet adsorption. J Hazard Mater. 179, 564-572.

38. Shirsath S.R., Hage A.P., Zhou M., Sonawane S.H., Ashokkumar M., 2011. Ultrasound assisted preparation of nanoclay Bentonite-FeCo nanocomposite hybrid hydrogel: A potential responsive sorbent for removal of organic pollutant from water. Desalination. 281, 429-437.

39. Mahdavinia G.R., Massoumi B., Jalili K., Kiani G., 2012. Effect of sodium montmorillonite nanoclay on the water absorbency and cationic dye removal of carrageenan-based nanocomposite superabsorbents. J Polym Res. 19, 9947-9959.

40. Pourjavadi A., Hosseini S.H., Seid F.i, Soleyman R., 2013. Magnetic removal of crystal violet from aqueous solutions using polysaccharide-based magnetic nanocomposite hydrogels. Polym Int. 62, 1038-1044.